Inorg. Chem. **2006**, *45*, 894–901

O-Atom-Transfer Oxidation of [Molybdenum(IV) Oxo{3,6-(acylamino)$_2$-1,2-benzenedithiolato}$_2$]$^{2-}$ Promoted by Intramolecular NH···S Hydrogen Bonds

Koji Baba,[†] Taka-aki Okamura,*[,‡] Chie Suzuki,[‡] Hitoshi Yamamoto,[‡] Tetsuo Yamamoto,[‡] Mitsuo Ohama,[‡] and Norikazu Ueyama*[,‡]

Chemical Analysis Research Center, National Institute for Agro-Environmental Sciences, Tsukuba, Ibaraki 305-8604, Japan, and Department of Macromolecular Science, Graduate School of Science, Osaka University, Toyonaka, Osaka 560-0043, Japan

Received September 1, 2005

Novel molybdenum dithiolene compounds having neighboring amide groups as models for molybdoenzymes, $(NEt_4)_2$-[$Mo^{IV}O${1,2-S_2-3,6-$(RCONH)_2C_6H_2$}$_2$] (R = CH_3, CF_3, *t*-Bu, Ph_3C), were designed and synthesized. The contributions of the NH···S hydrogen bond to the electrochemical properties of the metal ion and the reactivity of the O-atom-transfer reaction were investigated by a comparison with [$Mo^{IV}O(1,2\text{-}S_2C_6H_4)_2]^{2-}$. The $MoOS_4$ core of [$Mo^{IV}O${1,2-S_2-3,6-$(CH_3CONH)_2C_6H_2$}$_2]^{2-}$ shows no significant geometrical difference from that of [$Mo^{IV}O(1,2\text{-}S_2C_6H_4)_2]^{2-}$ in the crystal. The hydrogen bonds positively shifted the $Mo^{IV/V}$ redox potential and accelerated the reduction of Me_3NO.

Introduction

Recently, the studies of molybdenum or tungsten oxotransferase have been stimulated by X-ray analysis. The metal center in these metalloenzymes is bound to the dithiolene ligand included in pterin cofactors.[1−3] The bis-coordination of dithiolene to an oxidized Mo^{VI} form and a reduced Mo^{IV} form in a dimethyl sulfoxide (DMSO) reductase family was proposed by the combined results of resonance Raman,[4−6] magnetic circular dichroism,[7,8] and X-ray crystallographic analysis.[9−19]

Various monooxomolybdenum(IV)- and dioxomolybdenum(VI)-dithiolene complexes have been synthesized as models of these oxotransferases. These monooxomolybdenum(IV)-dithiolene complexes were also studied as model reactions for the metabolism of small molecules by O-atom transfer in molybdenum oxotransferases.[20−25]

* To whom correspondence should be addressed. E-mail: tokamura@chem.sci.osaka-u.ac.jp (T.-O.), ueyama@chem.sci.osaka-u.ac.jp (N.U.).

[†] National Institute for Agro-Environmental Sciences.

[‡] Osaka University.

(1) George, G. N.; Hilton, J.; Rajagopalan, K. V. *J. Am. Chem. Soc.* **1996**, *118*, 1113−1117.
(2) Bastian, N. R.; Kay, C. J.; Barber, M. J.; Rajagopalan, K. V. *J. Biol. Chem.* **1991**, *266*, 45−51.
(3) Bennett, B.; Charnock, J. M.; Sears, H. J.; Berks, B. C.; Thomson, A. J.; Ferguson, S. J.; Garner, C. D.; Richardson, D. J. *Biochem. J.* **1996**, *317*, 557−563.
(4) Kilpatrick, L.; Rajagopalan, K. V.; Hilton, J.; Bastian, N. R.; Stiefel, E. I.; Pilato, R. S.; Spiro, T. G. *Biochemistry* **1995**, *34*, 3032−3039.
(5) Garton, S. D.; Hilton, J.; Oku, H.; Crouse, B. R.; Rajagopalan, K. V.; Johnson, M. K. *J. Am. Chem. Soc.* **1997**, *119*, 12906−12916.
(6) Garton, S. D.; Temple, C. A.; Dhawan, I. K.; Barber, M. J.; Rajagopalan, K. V.; Johnson, M. K. *J. Biol. Chem.* **2000**, *275*, 6798−6805.
(7) Benson, N.; Farrar, J. A.; McEwan, A. G.; Thomson, A. J. *FEBS Lett.* **1992**, *307*, 169−172.
(8) Finnegan, M. G.; Hilton, J.; Rajagopalan, K. V.; Johnson, M. K. *Inorg. Chem.* **1993**, *32*, 2616−2617.
(9) Schneider, F.; Lowe, J.; Huber, R.; Schindelin, H.; Kisker, C.; Knablein, J. *J. Mol. Biol.* **1996**, *263*, 53−69.
(10) McAlpine, A. S.; McEwan, A. G.; Shaw, A. L.; Bailey, S. *J. Biol. Inorg. Chem.* **1997**, *2*, 690−701.
(11) Stewart, L. J.; Bailey, S.; Bennett, B.; Charnock, J. M.; Garner, C. D.; McAlpine, A. S. *J. Mol. Biol.* **2000**, *299*, 593−600.
(12) Bray, R. C.; Adams, B.; Smith, A. T.; Bennett, B.; Bailey, S. *Biochemistry* **2000**, *39*, 11258−11269.
(13) Li, H. K.; Temple, C.; Rajagopalan, K. V.; Schindelin, H. *J. Am. Chem. Soc.* **2000**, *122*, 7673−7680.
(14) Bray, R. C.; Adams, B.; Smith, A. T.; Richards, R. L.; Lowe, D. J.; Bailey, S. *Biochemistry* **2001**, *40*, 9810−9820.
(15) Czjzek, M.; Dos Santos, J. P.; Pommier, J.; Giordano, G.; Mejean, V.; Haser, R. *J. Mol. Biol.* **1998**, *284*, 435−447.
(16) Dias, J.; Than, M.; Humm, A.; Bourenkov, G. P.; Bartunik, H. D.; Bursakov, S.; Calvete, J.; Caldeira, J.; Carneiro, C.; Moura, J. J.; Moura, I.; Romao, M. J. *Structure* **1999**, *7*, 65−79.
(17) Ellis, P. J.; Conrads, T.; Hille, R.; Kuhn, P. *Structure* **2001**, *9*, 125−132.
(18) Arnoux, P.; Sabaty, M.; Alric, J.; Frangioni, B.; Guigliarelli, B.; Adriano, J. M.; Pignol, D. *Nat. Struct. Biol.* **2003**, *10*, 928−934.
(19) Bertero, M. G.; Rothery, R. A.; Palak, M.; Hou, C.; Lim, D.; Blasco, F.; Weiner, J. H.; Strynadka, N. C. *Nat. Struct. Biol.* **2003**, *10*, 681−687.

10.1021/ic051493h CCC: $33.50
Published on Web 12/15/2005

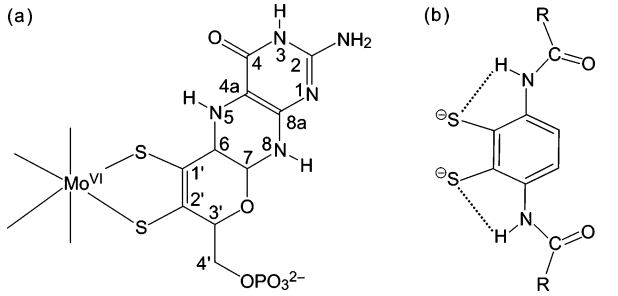

Figure 1. Proposed formation of the NH···S hydrogen bond in (a) the active center of DMSO reductase and (b) its model ligand (R = CH_3, CF_3, *t*-Bu, and Ph_3C).

The presence of a NH···S hydrogen bond between amide NH and Cys sulfur has been proposed in the active center of electron-transfer proteins, e.g., rubredoxin, [2Fe−2S] ferredoxins, [4Fe−4S] ferredoxins, and azurin. Various metal complexes having the NH···S hydrogen bond in a weakly polar solvent were studied as models of these electron-transfer proteins as well as Mo^{V} and Mo^{IV} complexes of arenethiolate containing an intramolecular NH···S hydrogen bond.[26] The NH···S hydrogen bond contributes to the positive shift of the redox potentials and the protection of the Fe−S bond from the dissociation with water or other thiols in [4Fe−4S] ferredoxin[27] and cytochrome P-450 model complexes.[28]

The NH···S hydrogen bond between the dithiolene and pterin ring NH is expected to exist in the active center of DMSO reductase as shown in Figure 1a.[29] A previous study on the chemical function of the intermolecular or intramolecular NH···S hydrogen bond in molybdenum(IV)-dithiolene complexes, $(n\text{-}Pr_4N)_2[Mo^{IV}O\{1,2\text{-}S_2C_2(CONH_2)_2\}_2]\cdot 0.5i\text{-}PrOH\cdot DMF$ (DMF = *N*,*N*-dimethylformamide), has revealed the facilitation of the O-transfer reaction.[30]

Monooxomolybdenum(IV) complexes of novel bulky 3,6-diacylamino-1,2-dithiolene ligands having NH···S hydrogen bonds were newly designed and synthesized (Figure 1b). An extremely bulky dithiolene ligand, 3,6-bis[(triphenylacetyl)-amino]-1,2-dithiolene, was designed for the monooxomolybdenum(IV) complex to have a slightly distorted square-pyramidal $Mo^{IV}OS_4$ core. The effects of intramolecular NH···S hydrogen bonds and the distorted conformation of the $Mo^{IV}OS_4$ core were examined in the following O-atom-transfer reaction (eq 1) as models of trimethylamine *N*-oxidase, a member of the DMSO reductase family.[15] We have already reported the short Communication about the complex with 3,6-bis[(triphenylacetyl)amino]-1,2-dithiolene ligands.[31]

$$[Mo^{IV}O\{1,2\text{-}S_2\text{-}3,6\text{-}(RCONH)_2C_6H_2\}_2]^{2-} + Me_3NO \rightarrow [Mo^{VI}O_2\{1,2\text{-}S_2\text{-}3,6\text{-}(RCONH)_2C_6H_2\}_2]^{2-} + Me_3N \quad (1)$$

Experimental Section

Materials. All procedures were carried out under an argon atmosphere. *N*,*N*-Dimethylacetamide, triethylamine, DMF, methanol, and acetonitrile were purified by distillation before use. Other reagents of commercial grade were used without further purification.

$\{1,2\text{-}S_2\text{-}3,6\text{-}(CH_3CONH)_2C_6H_2\}_2$. To a dimethylacetamide solution (5 mL) of $\{1,2\text{-}S_2\text{-}3,6\text{-}(NH_2)_2C_6H_2\}_2$[32] (100 mg, 0.29 mmol) including Et_3N (0.24 mL, 1.7 mmol) was slowly added acetyl chloride (0.12 mL, 1.7 mmol) at 0 °C. The yellow precipitate was collected and washed with methanol and diethyl ether. Yield: 130 mg (87%). Anal. Calcd for $C_{20}H_{20}N_4O_4S_4$: C, 47.23; H, 3.96; N, 11.01. Found: C, 46.37; H, 4.18; N, 10.66. ^{1}H NMR (DMSO-d_6): δ 9.98 (s, 4H), 7.18 (s, 4H), 1.96 (s, 12H).

$\{1,2\text{-}S_2\text{-}3,6\text{-}(CF_3CONH)_2C_6H_2\}_2$. This compound was prepared according to the same procedure as that described for $\{1,2\text{-}S_2\text{-}3,6\text{-}(CH_3CONH)_2C_6H_2\}_2$ except for use of trifluoroacetic anhydride and isolated in 88% yield as a yellow powder. Anal. Calcd for $C_{20}H_8N_4O_4S_4F_{12}$: C, 33.15; H, 1.11; N, 7.73. Found: C, 33.18; H, 1.38; N, 7.90. ^{1}H NMR (DMSO-d_6): δ 11.54 (s, 4H), 7.66 (s, 4H).

$\{1,2\text{-}S_2\text{-}3,6\text{-}(t\text{-}BuCONH)_2C_6H_2\}_2$. This compound was prepared by a method similar to that described above and isolated as a yellow powder in 70% yield. Anal. Calcd for $C_{32}H_{44}N_4O_4S_4$: C, 56.77; H, 6.55; N, 8.28. Found: C, 55.07; H, 6.27; N, 8.15. ^{1}H NMR (DMSO-d_6): δ 9.37 (s, 4H), 7.62 (s, 4H), 1.25 (s, 36H).

$\{1,2\text{-}S_2\text{-}3,6\text{-}(Ph_3CCONH)_2C_6H_2\}_2$. $K_2[1,2\text{-}S_2O_3\text{-}3,6\text{-}(NH_2)_2C_6H_2]\cdot 2H_2O$[32] (5.0 g, 11 mmol) and *n*-Bu_4NBr (8.0 g, 25 mmol) were suspended in water (250 mL). The mixture was extracted with dichloromethane (200 mL × 3). The combined organic layer was dried over Na_2SO_4. After removal of the solvent under reduced pressure, 7.4 g (81%) of $(n\text{-}Bu_4N)_2[1,2\text{-}(S_2O_3)_2\text{-}3,6\text{-}(NH_2)_2C_6H_2]$ was obtained as a yellow oil. To a chloroform solution (30 mL) of $(n\text{-}Bu_4N)_2[1,2\text{-}(S_2O_3)_2\text{-}3,6\text{-}(NH_2)_2C_6H_2]$ (1.0 g, 1.2 mmol) including Et_3N (0.84 mL, 6.0 mmol) was added slowly Ph_3CCOCl (0.90 g, 2.9 mmol), which was prepared from Ph_3COOH and thionyl chloride. The mixture was stirred overnight under reflux. The solution was then cooled to room temperature, washed with water (100 mL), and dried over Na_2SO_4. The solution was concentrated in volume to 5 mL, and then diethyl ether (30 mL) was added. The resulting white powder of $(n\text{-}Bu_4N)_2[1,2\text{-}(S_2O_3)_2\text{-}3,6\text{-}(Ph_3CCONH)_2C_6H_2]$ was collected and washed with diethyl ether. $(n\text{-}Bu_4N)_2[1,2\text{-}(S_2O_3)_2\text{-}3,6\text{-}(Ph_3CCONH)_2C_6H_2]$ (620 mg, 0.46 mmol) and *i*-PrSNa (380 mg, 3.9 mmol) were suspended in methanol (20 mL), and the mixture was refluxed for 12 h under Ar. Solvents were evaporated under reduced pressure. The residue was dissolved in dichloromethane (100 mL). The solution was washed consecutively with a saturated NaCl solution, 2% HCl, a saturated NaCl solution, 4% $NaHCO_3$, and a saturated NaCl solution; dried over Na_2SO_4; and concentrated in vacuo. The residual solid was dissolved in methanol (30 mL), and the solution was heated under reflux

(20) Boyde, S.; Ellis, S. R.; Garner, C. D.; Clegg, W. *J. Chem. Soc., Chem. Commun.* **1986**, 1541−1543.
(21) Yoshinaga, N.; Ueyama, N.; Okamura, T.; Nakamura, A. *Chem. Lett.* **1990**, 1655−1656.
(22) Sarkar, S.; Das, S. K. *Proc. Indian Acad. Sci. Chem. Sci.* **1992**, *104*, 437−441.
(23) Ueyama, N.; Oku, H.; Kondo, M.; Okamura, T.; Yoshinaga, N.; Nakamura, A. *Inorg. Chem.* **1996**, *35*, 643−650.
(24) Enemark, J. H.; Cooney, J. J.; Wang, J. J.; Holm, R. H. *Chem. Rev.* **2004**, *104*, 1175−1200.
(25) Lim, P. J.; Slizys, D. A.; Tiekink, E. R. T.; Young, C. G. **2005**, *44*, 114−121.
(26) Ueyama, N.; Okamura, T. A.; Nakamura, A. *J. Am. Chem. Soc.* **1992**, *114*, 8129−8137.
(27) Ueyama, N.; Yamada, Y.; Okamura, T.; Kimura, S.; Nakamura, A. *Inorg. Chem.* **1996**, *35*, 6473−6484.
(28) Ueyama, N.; Nishikawa, N.; Yamada, Y.; Okamura, T.; Nakamura, A. *J. Am. Chem. Soc.* **1996**, *118*, 12826−12827.
(29) Schindelin, H.; Kisker, C.; Hilton, J.; Rajagopalan, K. V.; Rees, D. C. *Science* **1996**, *272*, 1615−1621.
(30) Oku, H.; Ueyama, N.; Nakamura, A. *Inorg. Chem.* **1997**, *36*, 1504−1516.
(31) Baba, K.; Okamura, T.; Yamamoto, H.; Yamamoto, T.; Ohama, M.; Ueyama, N. *Chem. Lett.* **2005**, *34*, 44−45.
(32) Green, A. G.; Perkin, A. G. *J. Chem. Soc.* **1903**, *83*, 1201−1212.

overnight. The obtained yellow precipitate of {1,2-S_2-3,6-(Ph_3-CCONH)$_2C_6H_2$}$_2$ was collected by filtration and washed with methanol and diethyl ether. Yield: 130 mg (20%). Anal. Calcd for $C_{92}H_{68}N_4O_4S_4$: C, 77.72; H, 4.82; N, 3.94. Found: C, 76.86; H, 4.76; N, 4.02. IR (KBr): ν_{NH} 3361, 3345, 3316, $\nu_{C=O}$ 1704, 1685 cm^{-1}. ^1H NMR ($CDCl_3$): δ 9.03 (s, 4H), 7.76 (s, 4H), 7.33−7.09 (m, 60H).

(NEt_4)$_2$[$Mo^{IV}O${1,2-S_2-3,6-(CH_3CONH)$_2C_6H_2$}$_2$] (1). To a solution of (NEt_4)[$Mo^VO(SPh)_4$][33] (180 mg, 0.27 mmol) in a mixture of acetonitrile (10 mL) and water (1 mL) was added an acetonitrile (5 mL) solution of {1,2-S_2-3,6-(CH_3CONH)$_2C_6H_2$}$_2$ (140 mg, 0.28 mmol) and tetraethylammonium borohydride (44 mg, 0.30 mmol) as a solid. The mixture was stirred overnight, and then the solution was stripped to dryness. The residue was dissolved in acetonitrile (10 mL), and insoluble materials were filtered out. The filtrate was reduced to a volume of 2 mL, and diethyl ether (10 mL) was added dropwise to give a yellow powder that was recrystallized from methanol. Yield: 200 mg (85%). Anal. Calcd for $C_{68}H_{60}N_6O_5MoS_4$: C, 48.67; H, 7.06; N, 9.20. Found: C, 48.18; H, 7.35; N, 8.90. ^1H NMR (CD_3CN, anion): δ 8.76 (s, 4H), 7.74 (s, 4H), 2.12 (s, 12H). Absorption spectrum (DMF): λ_{max} (ϵ, M^{-1} cm^{-1}) 333 (5100), 380 (650), 452 (360) nm. IR (KBr): ν_{NH} 3346, $\nu_{Mo=O}$ 922 cm^{-1}. Raman: $\nu_{Mo=O}$ 921, ν_{Mo-S} 372 cm^{-1}.

(NEt_4)$_2$[$Mo^{IV}O${1,2-S_2-3,6-(CF_3CONH)$_2C_6H_2$}$_2$] (2). This complex was synthesized in a similar manner from (NEt_4)[$Mo^VO(SPh)_4$] (36 mg, 0.053 mmol), {1,2-S_2-3,6-(CF_3CONH)$_2C_6H_2$}$_2$ (40 mg, 0.055 mmol), and tetraethylammonium borohydride (9.0 mg, 0.062 mmol) in a mixed solvent of acetonitrile (7 mL) and argon-purged water (0.5 mL). Yield: 45 mg (77%). Anal. Calcd for $C_{36}H_{48}N_6O_5MoS_4F_{12}$: C, 39.42; H, 4.41; N, 7.66. Found: C, 39.36; H, 4.41; N, 7.71. ^1H NMR (CD_3CN, anion): δ 9.85 (s, 4H), 7.87 (s, 4H). Absorption spectrum (DMF): λ_{max} (ϵ, M^{-1} cm^{-1}) 351 (10 000), 416 (970) nm. IR (KBr): ν_{NH} 3309, $\nu_{Mo=O}$ 914 cm^{-1}. Raman: $\nu_{Mo=O}$ 920, ν_{Mo-S} 373 cm^{-1}.

(NEt_4)$_2$[$Mo^{IV}O${1,2-S_2-3,6-(*t*-BuCONH)$_2C_6H_2$}$_2$] (3). This complex was prepared by a similar procedure from (NEt_4)[$Mo^VO(SPh)_4$] (170 mg, 0.26 mmol), {1,2-S_2-3,6-(*t*-BuCONH)$_2C_6H_2$}$_2$ (180 mg, 0.26 mmol), and tetraethylammonium borohydride (40 mg, 0.28 mmol) in acetonitrile (15 mL) and argon-purged water (1 mL). Yield: 210 mg (80%). Anal. Calcd for $C_{48}H_{84}N_6O_5MoS_4$: C, 54.94; H, 8.07; N, 8.01. Found: C, 54.19; H, 8.01; N, 7.90. ^1H NMR (CD_3CN, anion): δ 9.18 (s, 4H), 7.89 (s, 4H), 1.32 (s, 36H). Absorption spectrum (DMF): λ_{max} (ϵ, M^{-1} cm^{-1}) 334 (4700), 370 (910), 448 (420) nm. IR (KBr): ν_{NH} 3345, $\nu_{Mo=O}$ 924 cm^{-1}. Raman: $\nu_{Mo=O}$ 922, ν_{Mo-S} 367 cm^{-1}.

(NEt_4)$_2$[$Mo^{IV}O${1,2-S_2-3,6-(Ph_3CCONH)$_2C_6H_2$}$_2$] (4a). To a solution of (NEt_4)[$Mo^VO(SPh)_4$] (100 mg, 0.15 mmol) in a mixture of acetonitrile (10 mL) and water (1 mL) was added with stirring an acetonitrile (5 mL) solution of {1,2-S_2-3,6-(Ph_3CCONH)$_2C_6H_2$}$_2$ (100 mg, 0.29 mmol) and tetraethylammonium borohydride (45 mg, 0.31 mmol) as a solid. The mixture was stirred overnight, resulting in the formation of a yellow powder. The solid was collected with filtration, washed with toluene, acetonitrile, and diethyl ether, and dried in vacuo. Yield: 230 mg (87%). Anal. Calcd for $C_{108}H_{108}N_6O_5MoS_4$: C, 72.30; H, 6.07; N, 4.68. Found: C, 69.26; H, 6.14; N, 5.06. ^1H NMR (DMF-d_7, anion): δ 9.34 (s, 4H), 7.97 (s, 4H), 7.49 (d, 24H), 7.37 (t, 24H), 7.26 (t, 12H). Absorption spectrum (DMF): λ_{max} (ϵ, M^{-1} cm^{-1}) 348 (12 000), 406 (sh) (980), 457 (530) nm. IR (KBr): ν_{NH} 3332, 3315, 3280, $\nu_{Mo=O}$ 928 cm^{-1}. Raman: $\nu_{Mo=O}$ 926, ν_{Mo-S} 366 cm^{-1}.

(PPh_4)$_2$[$Mo^{IV}O${1,2-S_2-3,6-(Ph_3CCONH)$_2C_6H_2$}$_2$] (4b). The complex was synthesized by a method similar to that described for **4** using PPh_4^+ salts. A suitable single crystal for X-ray analysis was obtained by a careful recrystallization from acetonitrile. The crystals included acetonitrile as a crystal solvent. Anal. Calcd for $C_{116}H_{108}N_4O_5P_2MoS_4$: C, 76.00; H, 4.92; N, 2.53. Found: C, 73.67; H, 5.08; N, 2.45.

Physical Measurements. UV−visible absorption spectra were recorded using a Shimadzu UV-3100 PC spectrometer in units of M^{-1} cm^{-1}. IR spectroscopic measurements in the solid state were done on a Jasco FT/IR-8300 spectrometer. Samples were prepared as KBr pellets. ^1H NMR spectra were obtained with a JEOL EX-270 in DMF-d_7, chroloform-*d*, or acetonitrile-d_3 at 27 °C. The measurements of cyclic voltammograms in a DMF solution were carried out on a BAS 100B/W instrument with a three-electrode system: glassy carbon working electrode, a Pt-wire auxiliary electrode, and a saturated calomel electrode (SCE). The scan rate was 100 mV s^{-1}. The concentration of the sample was 1 mM, containing 0.1 M of *n*-Bu_4NClO_4 as a supporting electrolyte. Potentials were determined at room temperature versus SCE as a reference electrode. All results were cross-referenced by using the ferrocene/ferrocenium couple as a calibrant. Raman spectra were measured at 298 K on a Jasco R-800 spectrophotometer equipped with a HTV-R649 photomultiplier, liquid-N_2-cooled CCD detector, and liquid-N_2-cooled InGaAs detector, respectively. Exciting radiation was provided by the Ar^+ ion (514.5 nm).

Kinetic Measurements. Reaction solutions containing the monooxomolybdenum(IV) complex and Me_3NO systems were monitored spectrophotometrically. A typical measurement was carried out using a 1-mm UV cell containing a solution of the monooxomolybdenum(IV) complex (1 mM) in DMF at 27 °C. After thermal equilibrium, a Me_3NO solution (ca. 100, 200, 300, 400, and 500 mM in DMF) was injected through a glass stopcock, and the contents were quickly mixed by shaking. The time dependence of the dioxomolybdenum(VI) absorbance was measured every 5 s. All calculations for the data analysis were performed at 531 nm for **1**, 506 nm for **2**, 532 nm for **3**, and 531 nm for **4a**, where (O and S) → Mo^{VI} charge-transfer bands appear in DMF.

X-ray Structure Determination. Single crystals of **1**·CH_3CN and **4b**·8CH_3CN were sealed in individual glass capillaries under an argon atmosphere for X-ray measurements. X-ray measurements were performed at 23 °C on a Rigaku AFC7R diffractometer equipped with a rotating-anode X-ray generator. The radiation used was Mo Kα monochromatized with graphite (0.710 69 Å). An empirical absorption correction was applied. The basic crystallographic parameters for **1**·CH_3CN and **4b**·8CH_3CN are listed in Table 1. Unit cell dimensions were refined by 25 reflections. The standard reflections were chosen and monitored with every 150 reflections and did not show any significant change. The structures were solved by the direct method (SIR92[34]) and refined by *SHELXL-97*.[35] Non-hydrogen atoms except acetonitrile molecules of **4b**·8CH_3CN were refined anisotropically. Hydrogen atoms were placed at the calculated positions. For **4b**, the position of the M=O moiety is disordered. The refinement of the multiplicity was converged to result in Mo1A:Mo1B = O5A:O5B = 0.827:0.173. The final difference Fourier map showed no significant feature. Atom scattering factors and dispersion corrections were taken from *International Tables for X-ray Crystallography*.[36]

(33) Boyd, I. W.; Dance, I. G.; Murray, K. S.; Wedd, A. G. *Aust. J. Chem.* **1978**, *31*, 279−284.

(34) Altomare, A.; Cascaano, G.; Giacovazzo, C.; Guagliardi, A.; Burla, M. C.; Polidori, G.; Camalli, M. *J. Appl. Crystallogr.* **1994**, *27*, 435−450.

(35) Sheldrick, G. M. *SHELXL-97*; University of Göttingen: Göttingen, Germany, 1997.

Scheme 1. Synthetic Routes for Monooxomolybdenum(IV) Complexes

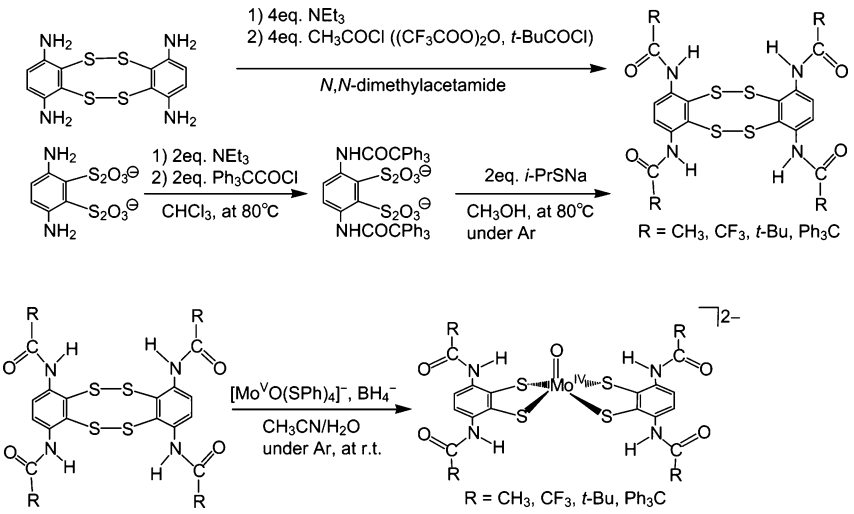

Table 1. Crystallographic Data for **1**·CH_3CN and **4b**·$8CH_3CN$

	1·CH_3CN	**4b**·$8CH_3CN$
empirical formula	$C_{38}H_{63}N_7O_5MoS_4$	$C_{156}H_{132}N_{12}O_5P_2S_4Mo$
fw	922.13	2540.86
cryst syst	monoclinic	monoclinic
space group	$P2_1/n$	$P2_1/n$
a, Å	15.189(4)	26.071(6)
b, Å	14.488(4)	14.944(2)
c, Å	21.159(4)	35.217(8)
β, deg	100.936(18)	93.81(2)
V, Å^3	4571(2)	13691(5)
Z	4	4
d_{calcd}, g cm^{-3}	1.340	1.233
μ, mm^{-1}	0.517	0.240
GOF (F^2)	1.03	1.00
R1[a] [$I > 2\sigma(I)$]	0.0729	0.0672
wR2[b] (all data)	0.1959	0.1731

[a] $R1 = \sum||F_o| - |F_c||/\sum|F_o|$. [b] $wR2 = \{\sum[w(F_o^2-F_c^2)^2]/\sum[w(F_o^2)^2]\}^{1/2}$.

Results and Discussion

Synthesis. $(NEt_4)_2[Mo^{IV}O\{1,2\text{-}S_2\text{-}3,6\text{-}(RCONH)_2C_6H_2\}_2]$ [R = CH_3 (**1**), CF_3 (**2**), *t*-Bu (**3**), Ph_3C (**4a**)] were obtained by the following reactions shown in Scheme 1. **4b** was synthesized for single-crystal structure X-ray analysis. A ligand-exchange reaction proceeds between a disulfide derivative and a Mo^V starting complex, $[Mo^VO(SPh)_4]^-$,[33] at the initial stage in a mixed solvent of acetonitrile and water at room temperature, and then the Mo^V species is reduced by a borohydride anion to give $[Mo^{IV}O\{1,2\text{-}S_2\text{-}3,6\text{-}(RCONH)_2C_6H_2\}_2]^{2-}$ in 50−80% yield. When only acetonitrile was selected as the solvent, tris(dithiolene) complexes were derived in high yield. However, even in such a case, $[Mo^{IV}\{1,2\text{-}S_2\text{-}3,6\text{-}(Ph_3CCONH)_2C_6H_2\}_3]^{2-}$ could not be derived because of the extremely bulky (triphenylacetyl)amino groups.

Crystal Structures of 1·CH_3CN and 4b·$8CH_3CN$. Figure 2 shows the molecular structures of the anion part of **1**·CH_3CN and **4b**·$8CH_3CN$. The structural parameters are listed in Table 2, compared with those of $(NEt_4)_2[Mo^{IV}O(1,2\text{-}S_2C_6H_4)_2]$ (**5**).[20] The mean N···S distances are 2.97 Å for **1**·CH_3CN and 2.96 Å for **4b**·$8CH_3CN$, respectively. The distances are short enough for the formation of NH···S hydrogen bonds. The Mo═O bond distances are 1.672(4) Å for **1**·CH_3CN and 1.682(4) Å for **4b**·$8CH_3CN$, which are similar to that (1.700(9) Å) of **5** with a large deviation. The mean Mo−S bond distances are 2.343 Å for **1**·CH_3CN and 2.386 Å for **4b**·$8CH_3CN$, close to that (2.388 Å) of **5**. Other structural parameters for **1**·CH_3CN and **4b**·$8CH_3CN$ are also not significantly different from those of **5**. The space-filling representation of **4b**·$8CH_3CN$ clearly shows that the bulky triphenyl groups form a unique conformation like two engaged gears to avoid their steric hindrance, as shown in Figure 2.

IR and Resonance Raman Spectra. Table 3 lists the IR bands in the amide NH region of **1**−**3**, and **4b** in the solid state, compared with the amide IR bands of the corresponding disulfides, $(S\text{-}2\text{-}RCONHC_6H_4)_2$ (R = CH_3, CF_3, *t*-Bu, Ph_3C) in CH_2Cl_2, as standard ν_{NH} stretching bands. The ν_{NH} band of **4b** is listed in the table, which is consistent with the molecular structure as shown in Figure 2b. The IR bands in the solid state depend on the packing of the crystal. Actually, **4a** exhibits three NH stretching bands, which reflect its poor crystallinity. These standard disulfides have no intermolecular NH···O═C hydrogen bond in a dilute solution (10 mM), where the amide NHs are free. The differences (over 30 cm^{-1}) in the NH band between the molybdenum complexes (**1**, **2**, **3**, and **4b**) and the corresponding disulfide indicate the formation of the NH···S hydrogen bond.

The resonance Raman bands of Mo═O and Mo−S in the solid state are compared with those of **5**, as listed in Table 4.[20] The shift of the Mo═O band in **1** from that of **5** is 19 cm^{-1} for the resonance Raman band and 17 cm^{-1} for the IR band. The Mo−S Raman band shifts by 16 cm^{-1} from that of **5**. Similar shifts were observed in **2**, **3**, and **4a** in the Mo═O and Mo−S stretchings. Because the crystal structure of **1**·CH_3CN and **4b**·$8CH_3CN$ did not show significant differences of the $MoOS_4$ core geometry compared with **5**, the NH···S hydrogen bond should contribute to the enhancement of the strength of both Mo═O and Mo−S bonds, which is different from the enhancement of only Mo═O by electron-withdrawing groups. The effect of the electron-

(36) Cromer, D. T.; Waber, J. T. *International Tables for X-ray Crystallography*; Kynoch Press: Birmingham, U.K., 1974; Vol. IV.

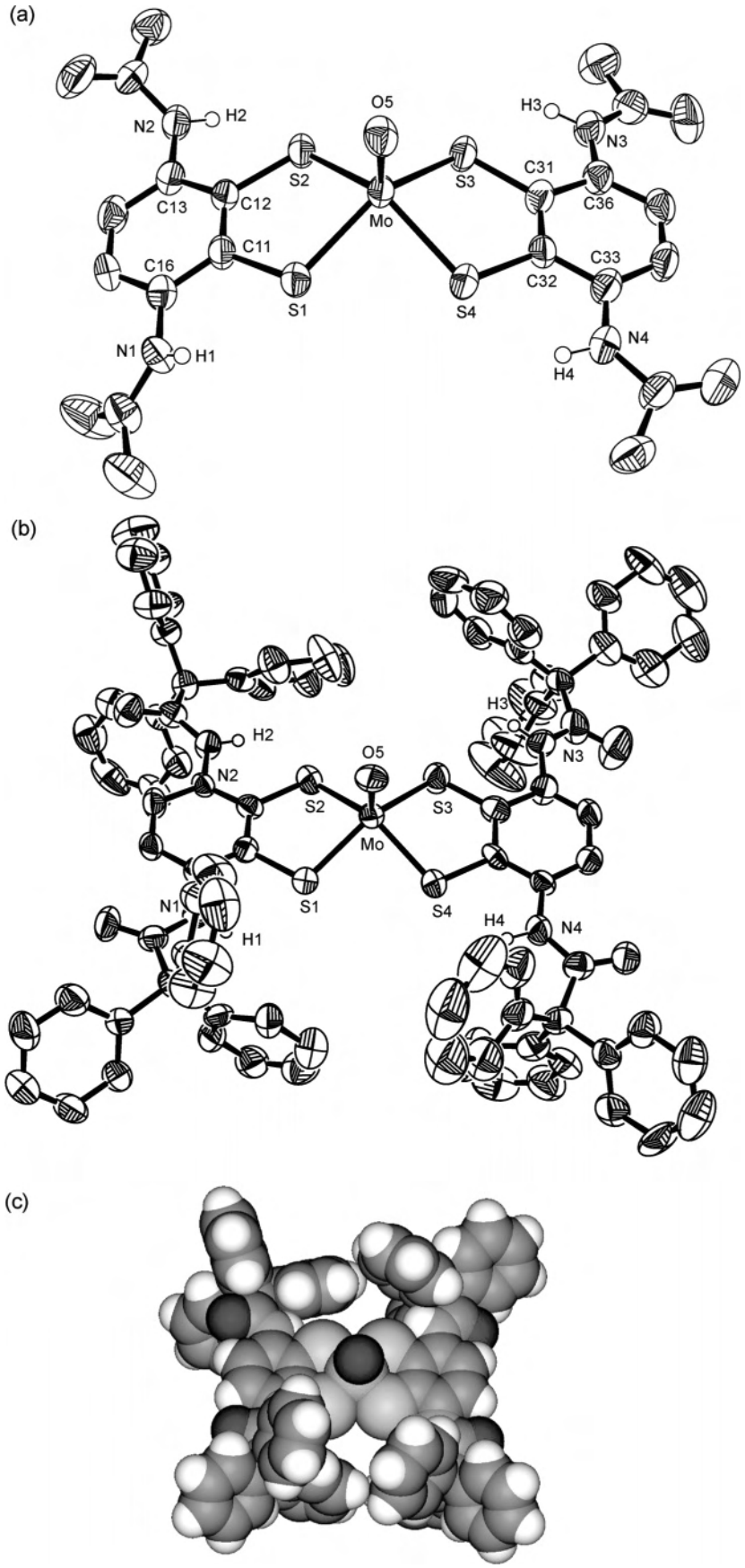

Figure 2. ORTEP drawing of (a) **1**·CH_3CN (anion part) and (b) **4b**·$8CH_3CN$ (anion part). Thermal motion is represented by 50% probability ellipsoids. The amide protons are placed on the calculated positions. (c) Space-filling view of **4b**·$8CH_3CN$.

Table 2. Comparison of Selected Structural Parameters (Å, deg) for the Anions of **1**·CH_3CN and **4b**·$8CH_3CN$ Compared with Those of **5**

	1·CH_3CN	**4b**·$8CH_3CN$	**5**[a]
Mo═O	1.672(4)	1.682(4)	1.700
Mo−S (mean)	2.384(2)	2.386(2)	2.388
S−C (mean)	1.783(6)	1.767(6)	1.766
O−Mo−S (mean)	108.4(2)	107.3(2)	108.2
S−Mo−$S_{intraligand}$	83.28(6)	82.92(6)	83.1
S−Mo−$S_{interligand}$	85.25(6)	87.00(6)	85.8
S−Mo−$S_{interligand}$	143.14(7)	145.44(7)	143.6
S···N (mean)	2.968	2.961	

[a] Reference 20. One of two structures in a unit cell was adopted.

Table 3. IR Bands of ν_{NH} (cm^{-1}) in **1**−**3** and **4b** in the Solid State Compared with Those of Corresponding Disulfides, $(S\text{-}2\text{-}RCONHC_6H_4)_2$ (R = CH_3, CF_3, *t*-Bu, Ph_3C) in a CH_2Cl_2 Solution

	Mo complexes[a]	$(S\text{-}2\text{-}RCONHC_6H_4)_2$[b]	$\Delta\nu_{NH}$
1	3346	3382	−36
2	3309	3358	−49
3	3345	3397	−52
4b	3291	3341	−50

[a] KBr pellet. [b] In CH_2Cl_2 (10 mmol L^{-1}).

Table 4. Raman and IR Bands of **1**−**4a** and **5** in the Solid State

	$\nu_{Mo=O}$ ($\Delta\nu_{Mo=O}$)[b] (cm^{-1})		ν_{Mo-S} ($\Delta\nu_{Mo-S}$)[b] (cm^{-1})
complex	Raman	IR	Raman
1	921 (+19)	922 (+17)	372 (+16)
2	920 (+18)	914 (+9)	373 (+17)
3	922 (+20)	924 (+19)	367 (+11)
4a	926 (+24)	928 (+23)	366 (+10)
5[a]	902	905	356

[a] Reference 20. [b] The shifts from the value of **5**.

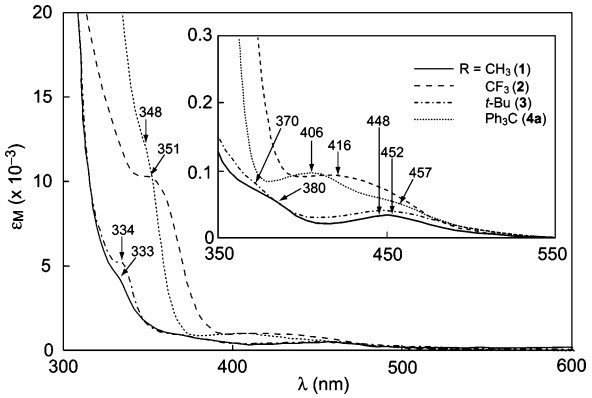

Figure 3. UV−visible spectra of **1**−**4a** in DMF at 27 °C.

withdrawing groups was reported to be the enhancement of the Mo═O frequency and the compensatory reduction of the Mo−S frequency.[37] The Mo═O (Mo−S) bands in $[Mo^{IV}O\{1,2\text{-}S_2C_2(CN)_2\}_2]^{2-}$ [37,38] with electron-withdrawing cyano groups and $[Mo^{IV}O\{1,2\text{-}S_2C_2(COOMe)_2\}_2]^{2-}$ [39] with less electron-withdrawing methoxycarbonyl groups are found at 948 (344) and 910 (393) cm^{-1}, respectively.

UV−Vis Spectra. Figure 3 shows the absorption spectra of **1**−**4a**. The spectra of **1** and **3** are similar to that of **5**, which shows absorption bands at 328, 385, and 452 nm. On the other hand, the spectra of **2** and **4a** are distinct from that of **5**. The spectral difference is presumably caused by the strong absorption of the ligands in **2** and **4a**. The bands in the region of 333−351 nm are ascribed to the ligand-to-metal charge-transfer (LMCT) band.[38] The difference of the LMCT bands between **1**−**4a** and **5** (328 nm) is not discussed in detail because of the absorption of the ligands. The d−d transition bands were observed at 448−457 nm for **1**, **3**, and **4a**, suggesting the absence of geometrical change in theses complexes and **5** (452 nm).[26] For **2**, a resolved d−d band in this region was not observed because it is overlapping with the broad band at 416 nm as a result of the absorption of the ligands.

Table 5. $Mo^{IV/V}$ Redox Potentials[a] of **1**−**4a** and **5** in DMF

complex	$E_{1/2}$	I_{pc}/I_{pa}	$\Delta E_{1/2}$[c]
1	−0.13	0.95	+0.25
2	+0.08	0.92	+0.46
3	−0.02	0.91	+0.36
4a	+0.03	0.96	+0.41
5[b]	−0.38		

[a] The concentration was 1 mM. Solutions contain 0.1 M *n*-Bu_4NClO_4. Potentials are estimated versus a SCE at a Pt working electrode with the scan rate of 100 mV s^{-1}. [b] Reference 20. [c] The shifts from the value of **5**.

Electrochemical Properties. Table 5 lists the redox potentials of **1**−**4a** and **5** for a quasi-reversible $Mo^{IV/V}$ couple in DMF. The redox potentials of **1**−**4a** are positively shifted by 0.25−0.46 V from that (−0.38 V vs SCE) of **5** without a NH···S hydrogen bond.[20] The large positive shifts (+0.46 and +0.41 V, respectively) of the redox potentials for **2** and **4a** are explained by the fact that the electron-withdrawing power of the CF_3 and Ph_3C groups strengthens the NH···S hydrogen bond through the amide group.[26] The reported positive shifts of the $Mo^{IV/V}$ redox potentials of $[Mo^{V}O\text{-}(S\text{-}2\text{-}RCONHC_6H_4)_4]^-$ (R = CH_3, CF_3, *t*-Bu) compared with $[Mo^{V}O(SPh)_4]^-$ are 0.45−0.56 V, which are much larger than those of **1**−**4a**. It is attributed to a suitable hydrogen bond formation between amide NH and sulfur pπ in a singly occupied molecular orbital for $[Mo^{V}O(S\text{-}2\text{-}RCONHC_6H_4)_4]^-$.[26] In the case of **1**−**4a**, the amide plane is perpendicular to the sulfur pπ in the highest occupied molecular orbital;[40] therefore, a strong interaction with pπ cannot be expected.

Reaction of Mo^{IV} Complexes with Trimethylamine *N*-Oxide. The O-atom-transfer oxidation of **1**−**4a** by Me_3NO was monitored using a UV−visible spectroscopic method. Table 6 lists the k_{obs} values for **1**−**4a** and **5**. Figure 4 shows the time course of the UV−visible spectra for the reaction between **1** (1 mM) and 2 equiv of Me_3NO (2 mM) in DMF at 27 °C. Two absorption maxima at 389 and 531 nm, which are assignable to the LMCT bands of $(NEt_4)_2\text{-}[Mo^{VI}O_2\{1,2\text{-}S_2\text{-}3,6\text{-}(CH_3CONH)_2C_6H_2\}_2]$,[38] indicate that the reaction proceeds with pseudo-first-order kinetics at the initial stage. The observed rate constant [$k_{obs} = (4.9 \pm 0.1) \times 10^{-3}$ s^{-1}] was obtained from the gradient. For 4, 6, and 10 equiv of Me_3NO, the rate constants were estimated similarly. Figure 5a plots the observed rate constants against the concentration

(37) Oku, H.; Ueyama, N.; Nakamura, A. *Inorg. Chem.* **1995**, *34*, 3667−3676.
(38) Oku, H.; Ueyama, N.; Kondo, M.; Nakamura, A. *Inorg. Chem.* **1994**, *33*, 209−216.
(39) Subramanian, P.; Burgmayer, S.; Richards, S.; Szalai, V.; Spiro, T. G. *Inorg. Chem.* **1990**, *29*, 3849−3853.
(40) Waters, T.; Wang, X. B.; Yang, X.; Zhang, L. Y.; O'Hair, R. A. J.; Wang, L. S.; Wedd, A. G. *J. Am. Chem. Soc.* **2004**, *126*, 5119−5129.

Table 6. Observed Initial Reaction Rate Constants (k_{obs}) in the O-Atom-Transfer Oxidation of **1**−**4a** and **5** by Me_3NO in DMF at 300 K

	k_{obs} (10^{-4} s^{-1})	
complex	$[Me_3NO] = 2$ mM	$[Me_3NO] = 10$ mM
1	49 ± 1	130 ± 1
2	35 ± 1	
3	3.3 ± 0.1	3.3 ± 0.1
4a	260 ± 10	1700 ± 400
5[a]	5.4 ± 0.1	57 ± 4

[a] Reference 20.

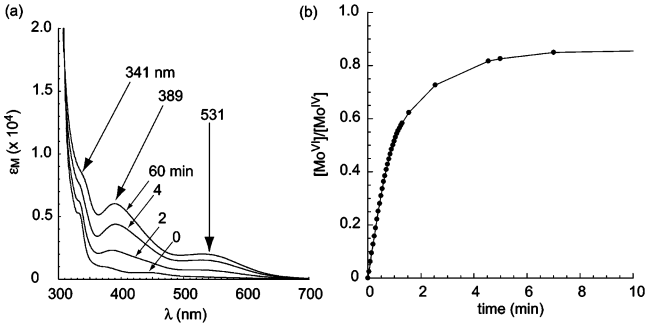

Figure 4. (a) UV−visible change (0, 2, 4, and 60 min) in the stoichiometric reduction of Me_3NO by **1** in DMF ($[Mo^{IV}] = 1$ mM, $[Me_3NO] = 2$ mM) at 27 °C. (b) Time dependence of the reduction monitored by the absorption maximum at 531 nm for the kinetic analysis.

of Me_3NO. The plot indicates that k_{obs} depends on the concentration of Me_3NO ($[Me_3NO]$) from 2 to 6 mM. From 6 to 10 mM, k_{obs} was independent of the concentration of Me_3NO. Previously, such saturation kinetics have been reported for $[Mo^{IV}O(1,2\text{-}S_2\text{-}3\text{-}Ph_3SiC_6H_3)_2]^{2-}$ with bulky substituents by Oku et al., whose rate constants were independent of $[Me_3NO]$ from 6 to 10 mM.[38] By detailed kinetic experiments, Oku et al. proposed the reaction mechanism including trans−cis rearrangement for $[Mo^{IV}O(1,2\text{-}S_2C_6H_4)_2]^{2-}$ (**5**) and $[Mo^{IV}O(1,2\text{-}S_2\text{-}3\text{-}Ph_3SiC_6H_3)_2]^{2-}$.[38] For **1**, the same mechanism is expected (Figure 5b). The binding of Me_3NO is rate-limiting at low Me_3NO concentrations, while the trans−cis rearrangement is rate-limiting at high Me_3NO concentrations.

Complex **2** showed k_{obs} values similar to those of **1** at the low concentration (2 mM) of Me_3NO but decomposed in the presence of excess of Me_3NO. The uncharacterized compound, which lacks amide protons, was detected by NMR spectrometry after the addition of 10 mM Me_3NO. Such a deprotonation of the CF_3CONH group by an oxidizing agent was also reported for $[Co^{II}(S\text{-}2\text{-}CF_3CONHC_6H_4)_4]^{2-}$.[41] The observed rate constant of **3** was independent of $[Me_3NO]$ from 2 to 10 mM.

Acceleration of Me_3NO Oxidation by a NH···S Hydrogen Bond. **1** with an intramolecular NH···S hydrogen bond has about 9 times larger k_{obs} values than **5** in the presence of 2 equiv of Me_3NO (Table 6). Previously, we reported that the Mo^{IV} complex with intermolecular NH···S hydrogen bonding accelerates Me_3NO reduction by about 6 times.[30] The acceleration by intramolecular NH···S hydrogen bonding of **1** is somewhat (1.5 times) larger than that by intermolecular NH···S hydrogen bonding. The stabilization of the Mo^{IV} state is expected from the positive shift of the redox potential by NH···S hydrogen bonding. However, NH···S hydrogen bonding decreases the electron density on the four S atoms, which leads to the prompt coordination of Me_3NO to the $Mo^{IV}OS_4$ core. k_{obs} of **3** was smaller than that of **1** or **2** because the bulkiness of the *t*-BuCONH groups exhibits saturation kinetics even at 2 equiv of Me_3NO. The retardation of the reaction by bulkiness of the ligands has already been reported in detail for $[Mo^{IV}O(1,2\text{-}S_2\text{-}3\text{-}Ph_3SiC_6H_3)_2]^{2-}$.[38] However, k_{obs} of bulky Ph_3CCONH-substituted dithiolene complex **4a** is about 48 times larger than that of nonsubstituted dithiolene complex **5** (1 mM) in the presence of 2 mM Me_3NO (Table 6). Such a large k_{obs} of **4a** increases to 0.17 s^{-1} in the presence of 10 mM Me_3NO and exhibits no saturation despite the extremely larger bulkiness than **3** and $[Mo^{IV}O(1,2\text{-}S_2\text{-}3\text{-}Ph_3SiC_6H_3)_2]^{2-}$. Additionally, the extremely large acceleration is not explainable only by the presence of the NH···S hydrogen bond. Therefore, a new reaction mechanism without trans−cis rearrangement was proposed (Figure 6) because rate limiting for complexes with bulky ligands is in the trans−cis rearrangement.[38] As mentioned in our recent Communication,[31] the congestion of the extremely bulky ligands in solution probably gives a transiently distorted conformation at the local energy minimum, where a dithiolene sulfur deviates from the cis position to the oxo ligand, which provides a vacant site for the attack of Me_3NO. The conformation is favorable for a cis attack by Me_3NO, resulting in the remarkably fast reaction.

Conclusions

The NH···S hydrogen bond in **1**−**4a** accelerates the reduction of Me_3NO to give the corresponding dioxomolybdenum(VI) complexes. In other words, the formation and cleavage of NH···S hydrogen bonds regulate the reactivity of the $Mo^{IV}O$ center. The active center of the native molybdoenzyme, the pyranopterin moiety, can adopt three different oxidation levels and has been considered to form a

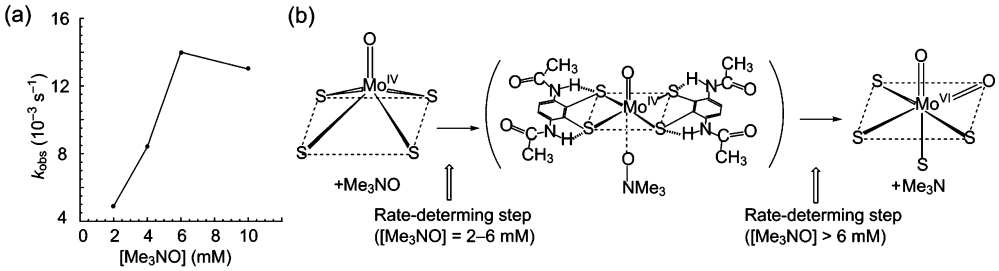

Figure 5. (a) Dependence of the observed rate constants for the reduction of Me_3NO by **1** on the Me_3NO concentration. (b) Proposed rate-determining steps depending on the Me_3NO concentration.

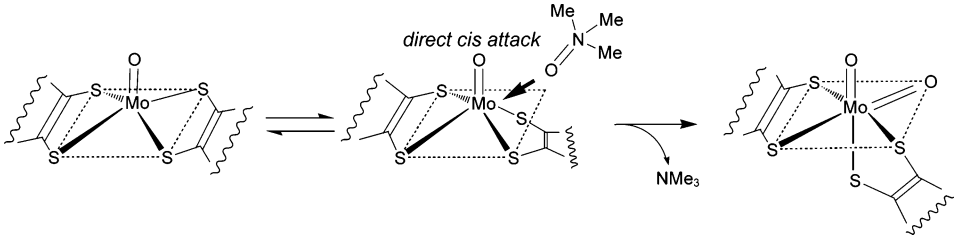

Figure 6. Proposed reaction mechanism via the cis attack of Me_3NO to **4a**.

ring-opening tautomeric structure.[42] In the redox or tautomerization process, the NH···S hydrogen bond (Figure 1a) should be broken or reformed because one of the tautomers has no H atom on N5.[42] Such redox or tautomeric reactions including scission/condensation reactions of the pyran ring presumably provide a way of controlling the activity of the molybdenum active center. The NH···S hydrogen bonds also positively shift the $Mo^{IV/V}$ redox potential, which prevents the Mo^{V} resting state from forming and allows catalytic cycles in native enzymes to smoothly proceed.

Acknowledgment. This work was supported by a Grant-in-Aid from the Ministry of Education, Culture, Sports, Science, and Technology, Japan.

Supporting Information Available: X-ray crystallographic files in CIF format. This material is available free of charge via the Internet at http://pubs.acs.org.

IC051493H

(41) Okamura, T.; Takamizawa, S.; Ueyama, N.; Nakamura, A. *Inorg. Chem.* **1998**, *37*, 18−28.
(42) (a) McNamara, J. P.; Joule, J. A.; Hillier, I. M.; Garner, C. D. *Chem. Commun.* **2005**, 177−179. (b) Enemark, I. M.; Garner, C. D. *J. Bioinorg. Chem.* **1997**, *2*, 817−822.